Sheared flow stabilization experiments in the ZaP flow Z pinch[a]

U. Shumlak,[b] B. A. Nelson, R. P. Golingo, S. L. Jackson, and E. A. Crawford
University of Washington, Aerospace and Energetics Research Program, Seattle, Washington 98195–2250

D. J. Den Hartog
Department of Physics, University of Wisconsin-Madison, Madison, Wisconsin 53706

The stabilizing effect of a sheared axial flow on the $m=1$ kink instability in Z pinches has been studied numerically with a linearized ideal magnetohydrodynamic model to reveal that a sheared axial flow stabilizes the kink mode when the shear exceeds a threshold. The sheared flow stabilizing effect is investigated with the ZaP (Z-Pinch) Flow Z-pinch experiment at the University of Washington. An axially flowing Z pinch is generated with a 1 m coaxial accelerator coupled to a pinch assembly chamber. The plasma assembles into a pinch 50 cm long with a radius of approximately 1 cm. An azimuthal array of surface mounted magnetic probes located at the midplane of the pinch measures the fluctuation levels of the azimuthal modes $m=1$, 2, and 3. After the pinch assembles a quiescent period is found where the mode activity is significantly reduced. Optical images from a fast framing camera and a ruby holographic interferometer indicate a stable, discrete pinch plasma during this time. Multichord Doppler shift measurements of impurity lines show a large, sheared flow during the quiescent period and low, uniform flow profiles during periods of high mode activity. Z-pinch plasmas have been produced that are globally stable for over 700 times the theoretically predicted growth time for the kink mode of a static Z pinch. The plasma has a sheared axial flow that exceeds the theoretical threshold for stability during the quiescent period and is lower than the threshold during periods of high mode activity. © *2003 American Institute of Physics.* [DOI: 10.1063/1.1558294]

I. INTRODUCTION

Some of the first attempts to achieve controlled thermonuclear fusion were based on the Z pinch. A large axial current was driven through a column of ionized gases to compress and heat the plasma to high density and temperature.[1–3] The Z pinch has appealing properties as a magnetic confinement configuration for a fusion reactor: the geometry is simple and linear, the maximum magnetic field is at the plasma surface and low external to the plasma, and the current producing the magnetic field dissipates energy in the plasma.[4,5] The equilibrium is described by a simple radial force balance between the azimuthal magnetic field generated by the axial plasma current and the plasma pressure,

$$(\mathbf{j} \times \mathbf{B})_r = (\nabla p)_r. \tag{1}$$

For the case of no applied magnetic fields, the equilibrium is given by

$$\frac{B_\theta}{\mu_o r} \frac{d(r B_\theta)}{dr} + \frac{dp}{dr} = 0. \tag{2}$$

The pinch plasma was observed to be violently unstable with growth times corresponding to Alfvén transit times. The instabilities were understood theoretically and experimentally as gross magnetohydrodynamic (MHD) modes with azimuthal mode numbers $m=0$ and $m=1$, sausage and kink modes, respectively.[6]

The MHD instabilities of a Z pinch can be stabilized. A close-fitting, conducting wall can be placed around the pinch plasma.[7] Image currents in the conducting wall develop to limit the growth of any plasma perturbations. However, the conducting wall must be placed too close to allow plasma temperatures of fusion interest.

By applying linear MHD stability analysis Kadomtsev derived an equilibrium that would be stable to the $m=0$ mode.[8] The mode can be stabilized if the pressure does not fall off too rapidly. Namely,

$$\frac{4\Gamma}{2+\Gamma\beta} \geq -\frac{d \ln p}{d \ln r}, \tag{3}$$

where Γ is the ratio of specific heats and $\beta = 2\mu_o p / B^2$ is a local measure of the ratio of plasma pressure to magnetic pressure. This condition must be satisfied everywhere in the plasma for stability against the $m=0$ mode. However, tailoring the pressure profile cannot stabilize the kink instability.

Both the sausage and kink instabilities can be stabilized by imbedding an axial magnetic field into the plasma. The condition for stability is found by applying an energy principle and is given by the Kruskal–Shafranov condition,[9,10]

$$\frac{B_\theta}{B_z} < \frac{2\pi a}{L}. \tag{4}$$

The equilibrium given in Eq. (2) is now modified. The radial force of the azimuthal magnetic field balances the plasma pressure and the magnetic pressure of the axial field. The Kruskal–Shafranov condition forces the design of short Z

pinches and limits the plasma current and the plasma pressure that can be stably achieved in a Z pinch. Furthermore, the addition of an axial magnetic field opens all of the magnetic field lines and connects all portions of the plasma to the electrodes. Parallel heat conduction is much faster than perpendicular heat conduction which is the case for closed field lines without the axial field. The combined constraints of short pinches and parallel heat losses led many early researchers to abandon the Z pinch as a magnetic confinement configuration.

Experiments have generated Z-pinch plasmas with inherent axial plasma flows exhibiting stable confinement for times much longer than the predicted growth times.[11,12] The possibility of using sheared flows to stabilize the Z pinch instead of axial magnetic fields has prompted recent theoretical and experimental efforts. A stable, high-density Z-pinch configuration would have profound implications for magnetic confinement thermonuclear fusion.[5,13,14]

II. SHEARED FLOW STABILIZATION THEORY

The effect of plasma flow on the MHD instabilities in a Z pinch has been investigated theoretically by applying linear stability analysis to the Z-pinch equilibrium.[15] The main conclusion is an axial plasma flow with a linear shear of $v_z/a > 0.1kV_A$ is required for stability of the marginally stable equilibrium given by Eq. (3) when the conducting wall is far away.

Nonlinear simulations have been performed to study the effect of a sheared flow on the stability of the $m=0$ mode in a Z pinch. The simulations were performed using the Mach2 code,[16] a time-dependent, resistive MHD code. An equilibrium is initialized with a uniform current density through the plasma and no current beyond the pinch radius a and with an axially periodic density perturbation of 1%. The equilibrium is also initialized with a plasma flow of constant shear inside the pinch $r<a$ and no shear beyond the pinch radius. The flow is maintained through the simulation only by inertia. The value of the flow shear is adjusted between simulations to investigate its effect on stability. Results showing the pressure contours are presented in Fig. 1 for a simulation that contains no flow (plots on the left) and a simulation that contains a flow such that $v_z(r=0)=0$ and $v_z(r=a)=0.2kaV_A$ (plots on the right). The figure shows the evolution of the pressure contours (a) at an intermediate time and (b) immediately before the static Z pinch disrupts. The initial states are not shown. The simulation of a static Z pinch shows a well developed $m=0$ instability. The Z-pinch plasma with a sheared axial flow shows a substantially less developed $m=0$ instability. The turbulence at the edge of the plasma is conjectured to result from a decrease in the flow shear at the edge due to numerical viscosity.

III. THE ZAP FLOW Z-PINCH EXPERIMENT

The ZaP (Z-Pinch) experiment at the University of Washington is used to investigate the effect of plasma flow on the stability of a Z pinch and to determine the possibility of confining hot plasmas in a simple Z-pinch configuration.[17] The experiment is designed to generate a Z-pinch plasma
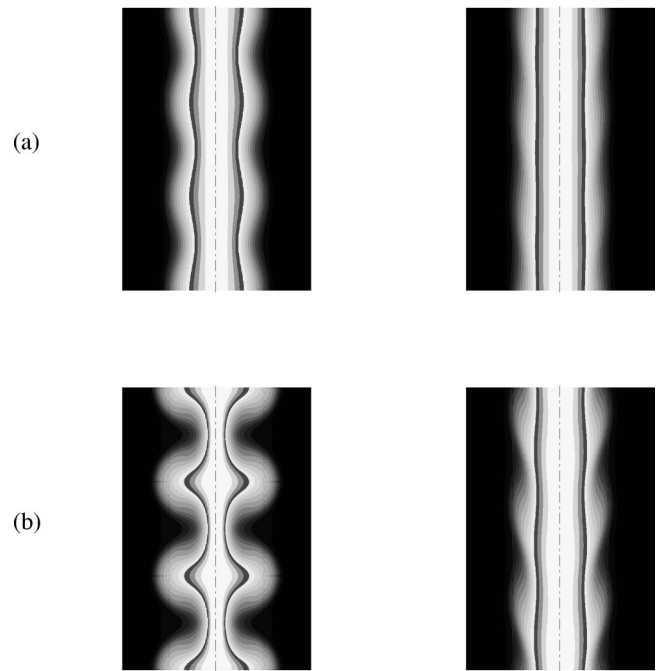

FIG. 1. Nonlinear simulation results showing the pressure contours in a Z pinch that contains no flow (plots on the left) and a Z pinch that contains a flow such that $v_z(r=0)=0$ and $v_z(r=a)=0.2kaV_A$ (plots on the right). The figure shows the evolution of the pressure contours (a) at an intermediate time and (b) immediately before the static Z pinch disrupts. The initial states are not shown.

with a large axial flow. The experiment is composed of a coaxial acceleration region connected to an assembly region. The experiment is initiated by the injection of neutral gas, usually hydrogen, with fast puff valves located in the middle of the 100 cm coaxial acceleration region. A capacitor bank power supply is discharged across the coaxial electrodes, ionizing the neutral gas, and accelerating the plasma. When the plasma reaches the end of the coaxial acceleration region, the plasma along the inner electrode moves radially inward and assembles along the axis in the 50 cm long assembly region. The plasma along the outer electrode continues to move axially and radially inward during the assembly of the Z pinch. The plasma finally connects between the end of the inner electrode and the outer electrode end wall forming a complete Z pinch. Inertia maintains the plasma flow state, and plasma is continually exiting from the coaxial accelerator and assembles into the pinch. The Z-pinch plasma formation in the ZaP experiment is shown schematically in Fig. 2.

Nonlinear simulations of the plasma formation in the ZaP experiment have been performed using the Mach2 code. While the code lacks a time-dependent ionization model, the simulations show qualitative agreement of the plasma formation described above. The code also shows quantitative agreement with the acceleration time and plasma densities measured in the experiment.

The coaxial accelerator has an inner electrode with a 5 cm radius and an outer electrode with a 10 cm radius which extends into the assembly region. A machine drawing of the ZaP experiment is shown in Fig. 3 identifying the relevant features. Recent modifications include a shaped end on the
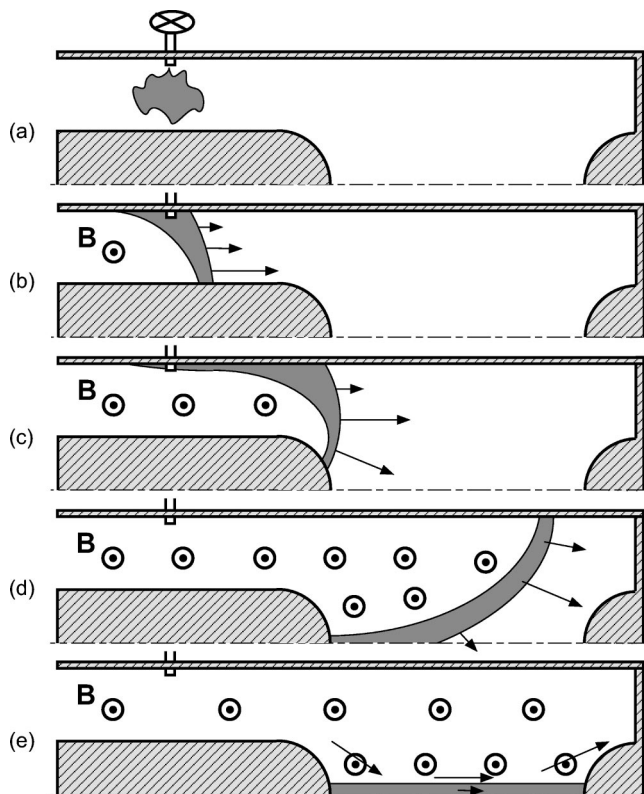
FIG. 2. Schematic representation of the Z-pinch plasma formation in the ZaP experiment: (a) neutral gas is injected into the annulus of the coaxial accelerator, (b) breakdown of the gas and current flows to accelerate the plasma axially, (c) plasma moves radially toward the axis at the end of the accelerator, (d) plasma assembles along the axis, (e) plasma is attached between the inner electrode and outer electrode end wall and inertia maintains the axial plasma flow.

inner electrode and an exit hole on the outer electrode end wall to reduce stagnation the plasma flow. For reference the pinch midplane is defined as $z=0$. The end of the inner electrode is at $z=-25$ cm, and the neutral gas is injected at $z=-75$ cm. The capacitor bank power supply is configured either for 28 kJ of stored energy at 9 kV or 46 kJ of stored energy at 8 kV. The plasma current peaks at 230 kA with a quarter cycle time of 28 μs and at 275 kA and has a quarter cycle time of 30 μs, respectively.

FIG. 4. Azimuthal magnetic field at several axial locations as measured by the surface mounted magnetic probes. The initial current sheet propagates down the acceleration region. Later in time the field values converge indicating a decrease in the plasma acceleration.

IV. EXPERIMENTAL RESULTS

The diagnostics on the ZaP experiment are designed to measure plasma evolution, equilibrium including flow, and stability.

A. Formation of a Z pinch with sheared flow

An axial array of 23 surface-mounted magnetic probes are installed in the outer electrode extending from $z=-120$ cm to 20 cm. The probes indicate the current distribution and the acceleration of plasma in the acceleration region. Time traces of the azimuthal magnetic field in the acceleration region is shown in Fig. 4. The initial current sheet propagates down the acceleration region and into the assembly region. A propagation speed of approximately 5 $\times 10^4$ m/s can be measured. Later in time the field values along the axial array converge indicating a decrease in radial current density and plasma acceleration.

The evolution of the electron number density in the plasma is determined from a two chord, visible He–Ne heterodyne quadrature interferometer. The chords can be placed at the pinch midplane in the assembly region or at locations in the acceleration region both downstream and upstream of the neutral gas injection plane. Figure 5 shows the average density along chords through the middle of the annulus be-
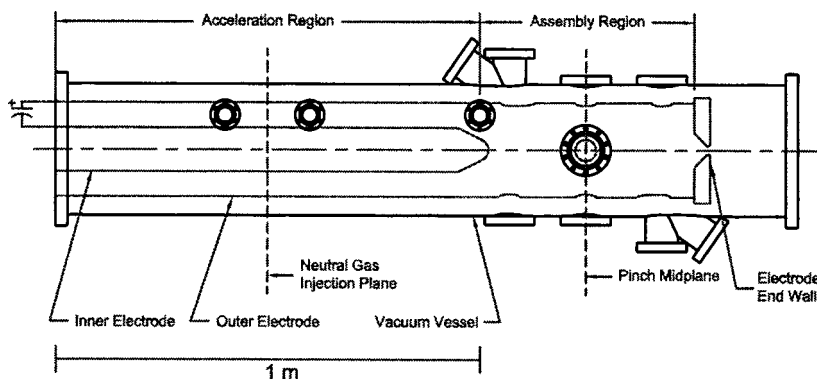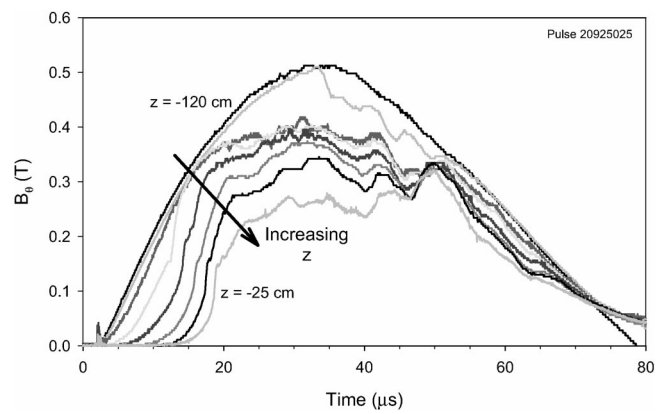

FIG. 3. Side view drawing of the ZaP experiment identifying the relevant features. The top and bottom ports in the assembly region are used for spectroscopic measurements of the Z-pinch plasma, and the side ports are used for obtaining images from the fast framing camera and measuring density of the Z-pinch plasma. The smaller side ports in the acceleration region are used to measure density during plasma acceleration.
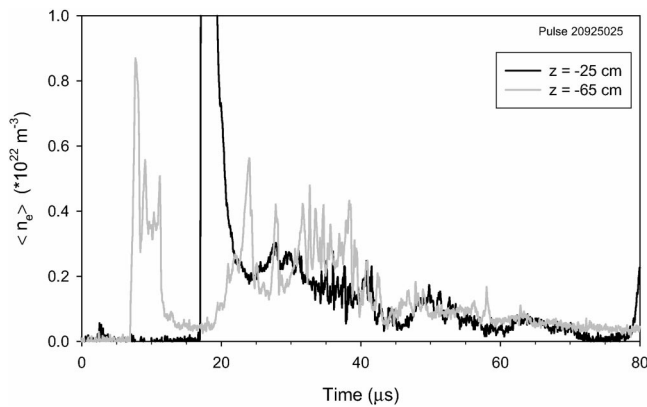
FIG. 5. Chord-averaged density in the acceleration region at $z = -25$ and -65 cm. After the initial plasma density rise the density remains at an elevated value before dropping to zero.

tween the electrodes of the coaxial accelerator at $z = -65$ and -25 cm. The data show the initial plasma sheet as it moves downstream past $z = -65$ and -25 cm. After the initial plasma density at $z = -25$ and -65 cm, the density remains at an elevated value before dropping toward zero.

After the plasma reaches the end inner electrode, the plasma begins to assemble along the axis into the Z-pinch plasma. Optical emission images obtained from a fast framing camera through the pinch midplane port are presented in Fig. 6. The images in the figure are taken every 1 μs and view the plasma through a notch pass filter which passes light with wavelengths between 500 and 600 nm. The plasma is viewed through a 4.7 cm diam hole through the outer electrode which provides a scale for spatial extent of the images. The images show the development of a stable structure centered in the experimental device.

When the He–Ne interferometer is located at the pinch midplane, the Z-pinch plasma density can be determined. One chord traverses the plasma along the geometric diameter, and a second chord is parallel to and 2 cm above the first chord. The plasma density is assumed to have spatially uniform values outside and inside the pinch. The radius of the pinch is determined from optical emission and spectroscopic data. The line-integrated densities measured from the two chords of interferometer data are combined with the pinch radius to compute the plasma density inside the pinch. The plasma electron number density is determined to be $10^{16} - 10^{17}$ cm^{-3} inside the pinch.

B. Evolution of the Z-pinch plasma

An azimuthal array of eight equally-spaced, surface-mounted magnetic probes are installed in the outer electrode at the pinch midplane. The probes measure the azimuthal magnetic field at surface of the outer electrode. The magnetic field values from the probe array are Fourier analyzed to determine the evolution of the low order azimuthal modes ($m = 1, 2, 3$) of the Z-pinch plasma. Typical data are plotted in Fig. 7 showing the time evolution of the $m = 1$ and $m = 2$ Fourier modes of the magnetic field. The average azimuthal magnetic field $B_0(t)$ is defined as the simple average of all eight surface magnetic probes at each time. The average
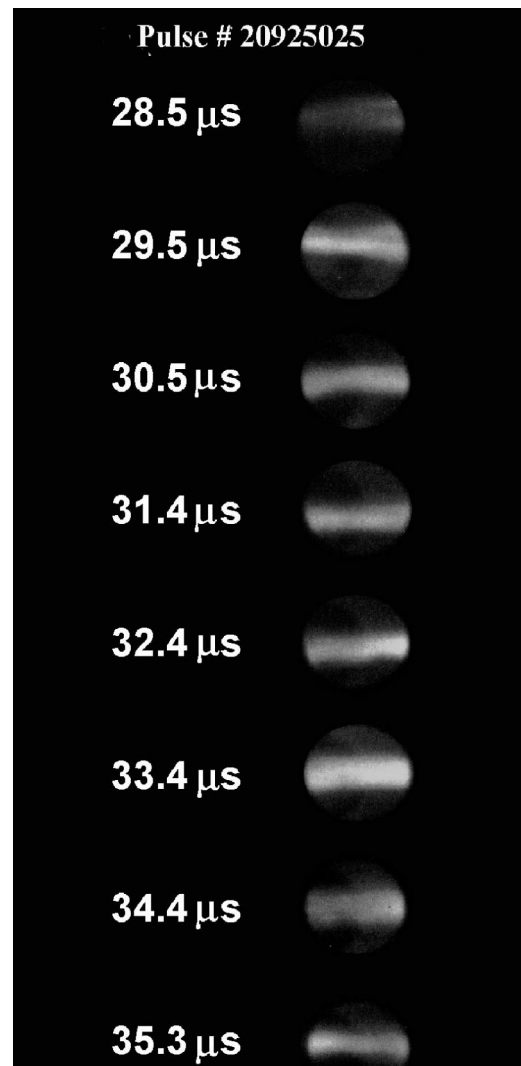

FIG. 6. Optical emission images of the plasma through the side port at the pinch midplane obtained with a fast framing camera equipped with a notch pass filter which passes light with wavelengths between 500 and 600 nm. The images show a stable structure centered in the experimental device. The plasma is viewed through a 4.7 cm diam hole through the outer electrode which provides a scale for spatial extent of the images.

azimuthal magnetic field is used to normalize the Fourier mode data at the pinch midplane, according to $\min(1, B_m(t)/\max(B_0(t), \epsilon))$, where $B_m(t)$ is the value of the m mode component of the azimuthal magnetic field and $\epsilon = 0.01$ T. The min and max functions are necessary to prevent divide by zero errors during periods of low signal levels. The $m = 3$ mode (not shown in the figure) is also analyzed and is lower than the $m = 2$ level at all times. The figure also shows the evolution of the plasma current for reference.

The plasma arrives at the pinch midplane at approximately 20 μs. Magnetic mode fluctuation data before this time are caused by signal noise and are not shown. The fluctuation levels of the asymmetric modes are high when the Z-pinch plasma is assembling. After the pinch has formed the fluctuation levels for both $m = 1$ and $m = 2$ change character for approximately 15 μs, from 31 to 46 μs. The change in character is identified by lower levels and de-
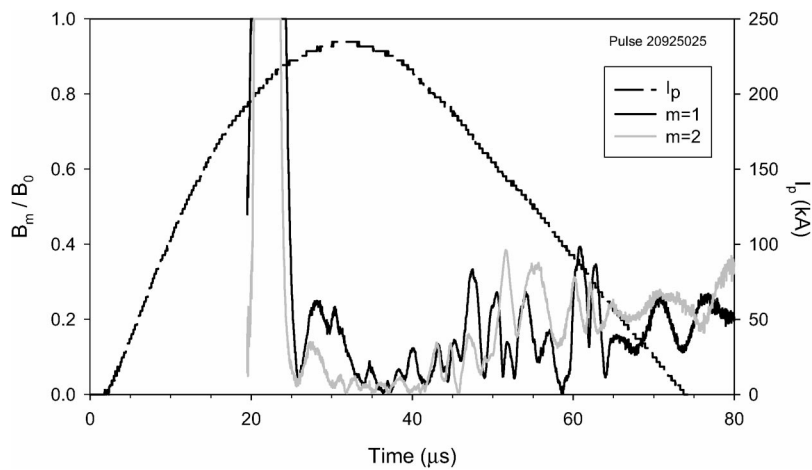
FIG. 7. Time evolution of Fourier components of the magnetic field fluctuation at the pinch midplane for $m = 1$ and $m = 2$ showing the quiescent period from 31 μs to 46 μs. The values are normalized to the average magnetic field value at the pinch midplane. The evolution of the plasma current (dashed curve) is included for reference.

creased frequency for the fluctuations. After this quiescent period the fluctuation levels then again change character, increase in magnitude and frequency, and stay high until the end of the plasma pulse.

The optical emission images in Fig. 6 show a structure that becomes brighter and remains stable for the duration of the data collection. The timing of the stable period corresponds to the stable time shown in the magnetic data. The images indicate the pinch is stable during this time against all $m = 0$ modes visible through the optical access hole. The pinch radius is estimated to be 1 cm. The images provide visual confirmation of the gross stability of the Z-pinch plasma. Furthermore, the images indicate the plasma is centered in the vertical plane with respect to the experimental geometry.

As stated previously, the plasma electron number density at the pinch midplane is determined to be 10^{16}–10^{17} cm^{-3} inside the pinch assuming a 1 cm pinch radius and a uniform density within the pinch radius. If it is assumed that no plasma current flows outside of the pinch radius, then the total plasma temperature can be determined from the magnetic field at the outer electrode and the density information. The magnetic field measured at the 10 cm outer electrode at the pinch midplane is 0.15–0.25 T. The magnetic field at the pinch radius is then 1.5–2.5 T. The total plasma temperature $(T_e + T_i)$ is estimated from force balance to be 150–200 eV.

Density profiles at a single time are obtained with a double-pass holographic interferometer that uses a pulsed ruby laser. The laser pulse length is less than 50 ns. The

integrated density profiles are deconvolved using an Abel method. Deconvolved density profiles are shown in Fig. 8 obtained (a) early in the plasma quiescent period at 22 μs and (b) late in the plasma quiescent period at 27 μs. The profiles show a discrete plasma pinch with a radius of 0.5 cm during assembly. The plasma density is peaked. Late the quiescent period the plasma pinch expands to 1 cm in radius and develops a hollow core structure. The values of the pinch radius and density are consistent with the data from the He–Ne interferometer. The hollow density structure suggests a hot plasma core has developed. The total plasma temperature profile can be calculated using force balance with the magnetic force and assuming a cold plasma outside of the pinch radius and no plasma current flows outside of the pinch radius. The total plasma temperature peaks at 60 eV early in the quiescent period and approximately 200 eV late in the quiescent period. However, the temperature values are sensitive to the assumed current distribution. More diagnostic information is needed before an accurate temperature profile can be determined.

Numerical simulations indicate the Z-pinch plasma is heated through compression from the larger radius of the coaxial accelerator to the pinch radius and by resistive heating once in the pinch. The evolution of the plasma temperature can be qualitatively determined by measuring the line radiation emission from different ionization states of impurity ions. A photomultiplier tube (PMT) is connected to the output of a 0.5 m spectrometer which views the plasma through fused-silica optics. The combination of the spec-
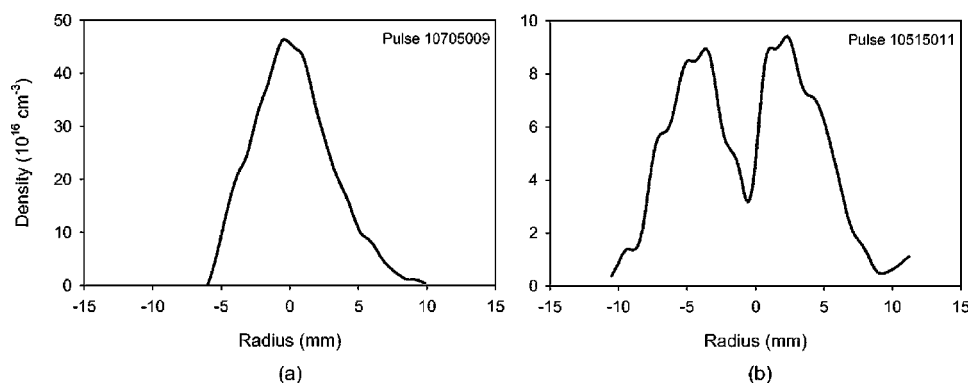

FIG. 8. Deconvolved density profiles from the holographic interferometer obtained (a) early in the plasma quiescent period at 22 μs and (b) late in the plasma quiescent period at 27 μs. A hollow structure is seen to develop indicating a hot plasma core.
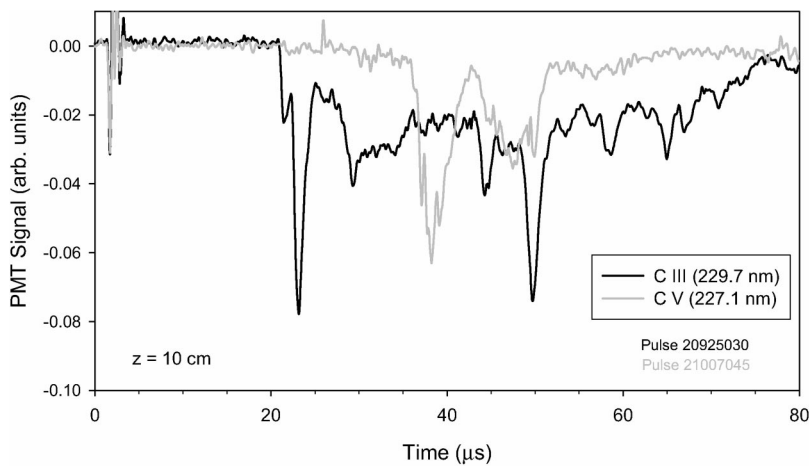
FIG. 9. Time-dependent emission of the C-III line at 229.7 nm and the $C-V$ line at 227.1 nm at $z=10$ cm. The appearance of $C-V$ emission late in the quiescent period is evident.

trometer grating and the output slit width limits the spectral view recorded by the PMT to full width at half maximum (FWHM) of 0.18 nm. The time-dependent emission of the C-III line at 229.7 nm and one of the $C-V$ triplet lines at 227.1 nm are recorded at two axial locations along the Z-pinch plasma. Data from the PMT measurement at $z = 10$ cm are shown in Fig. 9. The appearance of the $C-V$ emission late in the quiescent period indicates a progressive heating of the plasma. (For these pulses, the neutral hydrogen gas was doped with methane to increase the carbon impurity emission intensity.)

Impurity line radiation is also measured with a 0.5 m imaging spectrometer with an intensified charge-coupled device (ICCD) detector. The ICCD detector is set to a gating time of 100 ns and the trigger time is varied between plasma pulses. The spectrometer images 20 spatial chords through the plasma onto the ICCD camera using telecentric viewing telescopes.[18] The telescopes are connected to the spectrometer with a fiber bundle composed of 20 fused silica fibers. The chords image 20 points spaced 1.24 mm apart along a diameter through the pinch. Optical access to the midplane is provided through the radial viewports and oblique viewports positioned at a 35° angle to the plasma column, as shown in Fig. 3. The presence of the $C-V$ emission is confirmed with this diagnostic. The chord with the largest amplitude is interpreted as the location of the plasma center. The measured $C-V$ triplet at 227.1, 227.7, and 227.8 nm is fit with a temperature broadened Gaussian with the predicted central wavelengths and relative intensities. An ion temperature of 170 eV provides the best fit.

Velocity profiles are determined by measuring the Doppler shift of impurity line radiation. The velocity of the impurity ions are assumed to be representative of the velocity of the main plasma ions.[19,20] The assumption is supported by the relatively high plasma density which has an ion collision time of approximately 200 ns. Doppler shifts are calculated by viewing the plasma through the oblique viewport with the ICCD spectrometer. The oblique view has a directional component along the axis and, therefore, is sensitive to Doppler shifts from axial flows. The ICCD detector is set to a gating time of 1 μs and the trigger time is varied between plasma pulses. Figure 10 shows the output from the ICCD spectrom-

eter tuned to the C-III line at 229.7 nm. The trigger time for the ICCD is 30 μs which is during the quiescent period. The data show a shift of the C-III line being emitted from the central plasma, chords 5–18, and a lesser shift of the line being emitted from the edge plasma, chords 1 and 20. Since the bottom oblique viewport is being used, the plasma has a component of the axial velocity that is moving towards the viewport and produces the expected blueshift.

After the quiescent time the plasma flow velocity is significantly reduced. Figure 11 shows the output from the ICCD spectrometer tuned to the C-III line at 229.7 nm and viewing the plasma through the oblique viewport. The trigger time for the ICCD is 38 μs which is after the quiescent period and when the magnetic mode activity is high. The spectra for all of the spatial locations are centered on the 229.7 nm reference line in the figure. The peaks are broader indicating random plasma motion and plasma heating due to flow stagnation on the electrode end wall, identified in Fig. 3.

When the edges of the emissivity profile are seen, the data can be deconvolved to provide profiles with an improved spatial dependence.[21] An accurate deconvolution is not possible without simultaneous data to identify the edge
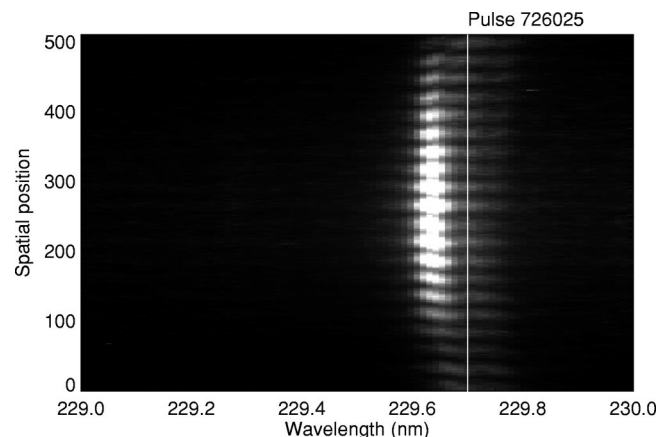

FIG. 10. Chord-integrated C-III line (229.7 nm) emission at 30 μs with a 1 μs gate obtained with the ICCD spectrometer showing the Doppler shift of the impurity line in the core of the pinch and a smaller shift towards the edge of the plasma. The solid line is positioned at 229.7 nm for reference.
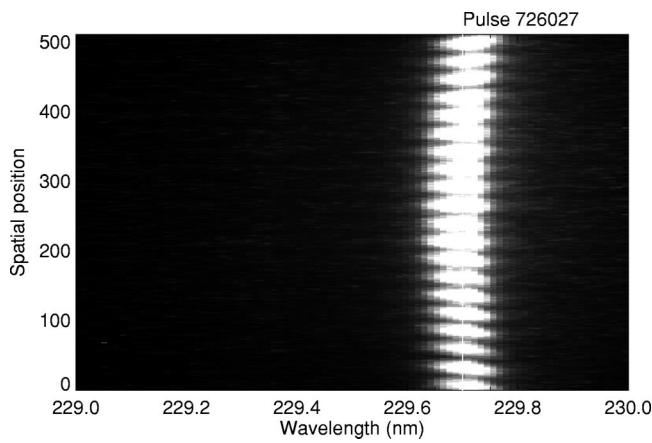
FIG. 11. Chord-integrated C-III line (229.7 nm) emission at 38 μs with a 1 μs gate obtained with the ICCD spectrometer showing a negligible Doppler shift of the impurity line. The solid line is positioned at 229.7 nm for reference.

FIG. 13. Compilation of three pulses of the magnetic field fluctuation at the pinch midplane for the $m=1$ mode showing the quiescent period from 22 μs to 38 μs. The shaded regions indicate the times during which Doppler shift spectra were recorded.

and center of the plasma. However, an approximate velocity profile can be determined by fitting the chord integrated data with shifted and broadened Gaussian functions. Typically, deconvolutions are not possible for data obtained outside of the quiescent period. To allow for a meaningful comparison, approximate axial velocity profiles are shown in Fig. 12. The data were obtained during the pinch assembly, during the quiescent period, and during the high fluctuation period. A compilation of the magnetic field fluctuation at the pinch midplane for the $m=1$ mode is shown in Fig. 13 for three pulses corresponding to the pulses used for the velocity profiles. A quiescent period from 22 μs to 38 μs is evident. The shaded regions in the figure indicate the times during which Doppler shift spectra were recorded.

During the pinch assembly the magnetic fluctuation level is high and the plasma axial velocity profile is uniform with a value of approximately 4×10^4 m/s. During the quiescent
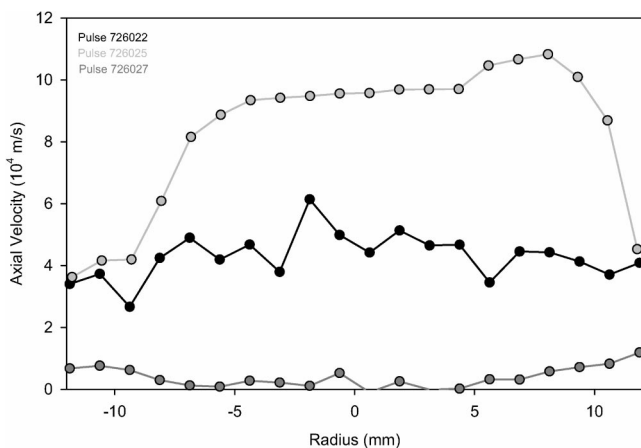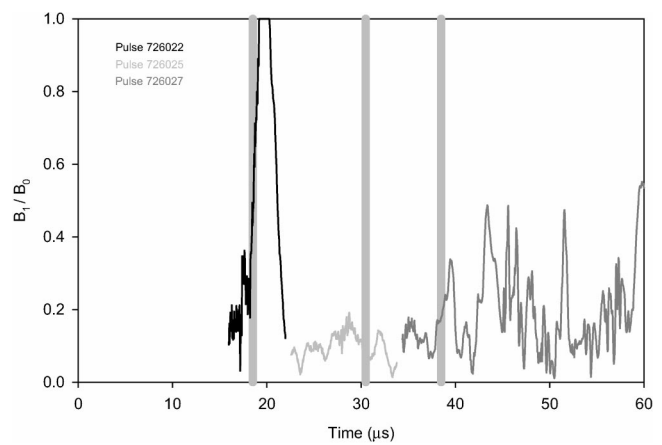

FIG. 12. Plasma axial velocity profiles based on the C-III line at 229.7 nm as a function of geometric radius obtained during the pinch assembly, during the quiescent period, and during the high fluctuation period. (The times are indicated in Fig. 13.) The plasma flow is peaked with a large shear at the edge during the quiescent period. The plasma flow is low and uniform during pinch assembly and after the quiescent period. The data have been fit with shifted Gaussians but not deconvoluted to allow for a uniform comparison.

period the magnetic fluctuation level is low and the plasma axial velocity profile is peaked with a large shear at the edge. The velocity profile shows a large axial velocity in the inner core of the pinch to be 10^5 m/s. The velocity remains relatively uniform in the inner core and then drops off to a lower value of 4×10^4 m/s towards the edge of the pinch. After the quiescent period the magnetic fluctuation level is high and the plasma axial velocity profile is low with a maximum velocity of approximately 10^4 m/s.

V. DISCUSSION AND COMPARISON TO THEORY

During the quiescent period the plasma flow is organized into a profile that has a large radial shear of the axial velocity. The shear is maximum close to the plasma edge. After the quiescent period the plasma becomes turbulent and the flow velocity is mostly uniform with a maximum considerably less than during the quiescent period.

The measured axial flow shear can be compared to the required threshold predicted by linear theory. Experimental plasma values at the peak plasma current are used for the comparison. The magnetic field at the outer electrode is measured to be 0.18 T for a magnetic field value at the characteristic pinch radius $B_a = 1.8$ T assuming zero plasma current density for $r > a$. The electron number density in the pinch is measured to be $n = 9 \times 10^{16}$ cm^{-3}. The Alfvén velocity is $V_A = B_a / \sqrt{\mu_o M_i n} = 1.3 \times 10^5$ m/s where M_i is the mass of a hydrogen ion. The growth rates of the $m=0$ and $m=1$ modes are approximately $k V_A$ assuming a static plasma. For the case of $ka = \pi$ the growth time would be 24 ns for a static Z-pinch plasma with the magnetic field strength and density measured on the ZaP experiment. The required axial velocity shear for stability according to the shear flow stabilization theory presented in Ref. 15 is 4.2×10^6 s^{-1}.

The experimental results show a stable period of 17 μs which is over 700 growth times. The experimentally measured axial velocity shear is 1.9×10^7 s^{-1} during the stable period and approximately zero afterwards when the magnetic mode fluctuations are high. The correlation of the experi-

mental stability data with the plasma flow measurements is consistent with the shear flow stabilization theory presented in Ref. 15.

A coincidental relation has been experimentally measured. Magnetic fluctuations are low when a sheared axial flow is present, and the magnetic fluctuations are high when the shear is reduced. However, at this point a causal relation cannot be determined. It has not been determined that the decrease in the plasma velocity shear leads to the increase in the magnetic fluctuations.

The plasma density in the accelerator region, shown in Fig. 5, remains at an elevated level until 42–45 μs. The magnetic field distribution in the accelerator region, shown in Fig. 4, indicates a Lorentz force that remains approximately constant once established from 25 to 45 μs. At that time the magnetic field values converge indicating the accelerating force has decreased significantly. Shortly after this time, the quiescent period ends. It is conjectured the plasma source has been exhausted and the plasma flow in the Z-pinch stagnates.

VI. CONCLUSIONS

The ZaP experiment has generated Z-pinch plasmas with an axial plasma flow that is sheared in the radial direction. Magnetic fluctuations are low when a sheared plasma flow is present. The magnetic fluctuations are large when the plasma flow shear is lower, during the initial pinch assembly and after the quiescent period. The experimental measurements indicate a Z-pinch plasma that becomes progressively hotter during the quiescent period. The experimental evidence is consistent with the theory that gross MHD modes of the Z pinch can be stabilized with a sufficiently sheared axial plasma flow. The sheared flow stabilization of the Z pinch has important implications for the flow Z pinch. A flow Z pinch designed with a sheared flow could make a simple steady-state fusion device, such as described in Ref. 14. Additionally the flow stabilization effect may be applied to other magnetic confinement configurations to reduce the amount of magnetic shear required for gross plasma stability.

[1] W. H. Bennett, Phys. Rev. **45**, 890 (1934).
[2] A. S. Bishop, *Project Sherwood* (Addison–Wesley, Reading, 1958).
[3] W. A. Newcomb, Ann. Phys. (N.Y.) **10**, 232 (1960).
[4] R. J. Bickerton, Nucl. Fusion **20**, 1072 (1980).
[5] C. W. Hartman, G. Carlson, M. Hoffman, R. Werner, and D. Y. Cheng, Nucl. Fusion **17**, 909 (1977).
[6] A. A. Ware, Nucl. Fusion Suppl. **3**, 869 (1962).
[7] R. R. John, S. Bennett, and J. F. Connors, AIAA J. **1**, 2517 (1963).
[8] B. B. Kadomtsev, *Reviews of Plasma Physics* (Consultants Bureau, New York, 1966), Vol. 2, p. 153.
[9] M. D. Kruskal and M. Schwarzschild, Proc. R. Soc. London, Ser. A **223**, 348 (1954).
[10] V. D. Shafranov, At. Energ. **5**, 38 (1956).
[11] A. A. Newton, J. Marshall, and R. L. Morse, in *Proceedings of the Third European Conference on Controlled Fusion and Plasma Physics*, Utrecht, 1969 (Wolters-Noordhoff, Groningen, 1969), p. 119.
[12] V. G. Belan, S. P. Zolotarev, V. F. Levahov, V. S. Mainashev, A. I. Morozov, V. L. Podkovyrov, and Yu. V. Skvortsov, Sov. J. Plasma Phys. **16**, 96 (1990).
[13] C. W. Hartman, J. L. Eddleman, R. Moir, and U. Shumlak, Fusion Technol. **26**, 1203 (1994).
[14] C. W. Hartman, J. L. Eddleman, A. A. Newton, L. J. Perkins, and U. Shumlak, Comments Plasma Phys. Controlled Fusion **17**, 267 (1996).
[15] U. Shumlak and C. W. Hartman, Phys. Rev. Lett. **75**, 3285 (1995).
[16] R. E. Peterkin, Jr., M. H. Frese, and C. R. Sovinec, J. Comput. Phys. **140**, 148 (1998).
[17] U. Shumlak, R. P. Golingo, B. A. Nelson, and D. J. Den Hartog, Phys. Rev. Lett. **87**, 205005 (2001).
[18] D. J. Den Hartog and R. P. Golingo, Rev. Sci. Instrum. **72**, 2224 (2001).
[19] R. D. Benjamin, J. L. Terry, and H. W. Moos, Phys. Rev. A **41**, 1034 (1990).
[20] W. L. Rowan, A. G. Meigs, R. L. Hickok, P. M. Schoch, X. Z. Yang, and B. Z. Zhang, Phys. Fluids B **4**, 917 (1992).
[21] R. P. Golingo and U. Shumlak, "A spatial deconvolution technique to obtain velocity profiles from chord integrated spectra," Rev. Sci. Instrum. (in press).